

# Antiproliferative Activity of Biogenic Silver Nanoparticles Synthesized from *Leonotis nepetifolia* (L) on Human Cancer Cell lines

M. N. L. C. HARIKA AND PARVATANENI RADHIKA\*

Department of Biochemistry, Andhra University, Visakhapatnam 530003, Andhra Pradesh, India

Harika *et al.*: Antiproliferative Activity of Silver Nanoparticles from *Leonotis nepetifolia* (L.)

Currently, nanobiotechnology is the growing science in the field of medicine employing silver nanoparticles to deliver drugs to target cancer cells and proved to be potential anticancer agents. In this study, silver nanoparticles were synthesized using leaf extract of *Leonotis nepetifolia* (L). Gas chromatography-mass spectrometry data showed a total of 13 phytochemical constituents identified from ethanolic leaf extract of *Leonotis nepetifolia* (L). The effect of physicochemical factors such as the reaction time, temperature, concentration of Silver nitrate, concentration of leaf extract and pH in the synthesis of silver nanoparticles. For biosynthesis, the optimal conditions were 1 mM silver nitrate, 0.1 ml of leaf extract at 80° for 90 min. Ultra violet-visible spectroscopy, field emission scanning electron microscopy; high-resolution transmission electron microscopy and various techniques characterized the synthesized AgNPs. The silver nanoparticles obtained had absorbance maxima at 398 nm, were spherical in shape, had an average particle size of 11.32 nm, polydispersity index 0.44, the zeta potential of  $-23.7 \pm 5.69$  mv and were crystalline. A cytotoxicity study was conducted on two human cancer cell lines, pancreatic and ovarian, using sulforhodamine B assay. We had compared the cytotoxicity of biogenic silver nanoparticles with that of synthetic silver nanoparticles. Treatment of pancreatic and ovarian with different concentrations of silver nanoparticles inhibited the cell viability with half maximal inhibitory concentration values of 25.4  $\mu\text{g/ml}$  and 23.9  $\mu\text{g/ml}$ . In contrast, silver nanoparticles inhibited cell viability with half maximal inhibitory concentration values of 48.2  $\mu\text{g/ml}$  and 42  $\mu\text{g/ml}$ , which were statistically significant ( $p < 0.001$ ), when compared with that of doxorubicin and Camptothecin. *Leonotis nepetifolia* mediated silver nanoparticles effectively reduced the proliferation of pancreatic and ovarian cancer cell lines than that of synthetic nanoparticles.

**Key words:** Nanobiotechnology, silver nanoparticles, *Leonotis nepetifolia*, sulforhodamine B assay, pancreatic cell lines, ovarian cell lines

In recent years, there have been major developments in nanotechnology. Nanobiotechnology deals with natural or biomimetic systems intending to develop nanoscale structures. It gained a vital role in the early recognition of diseases and treatment<sup>[1]</sup>. Metal nanoparticles able to bind diverse molecules to their surface was due to their relative surface area and size, making them ideal transport vehicles capable of penetrating cell and tissue barriers<sup>[2]</sup>. Nanoscale structures and materials such as nanofibers, colloidal nanoparticles, nanorods, nanowires, nanotubes and nanozymes have been investigated in many areas such as food safety, biosensing, molecular imaging, delivery of drugs, tissue engineering and anticancer treatment<sup>[3-5]</sup>. Numerous investigations

have shown that the biogenic Silver Nanoparticles (AgNPs) exhibited their therapeutic role in cancer as anticancer agents<sup>[6]</sup>. AgNPs were toxic to the cells, which can lead to damage of deoxyribonucleic acid, generation of reactive oxygen species, mitochondrial damage and apoptotic induction<sup>[7,8]</sup>.

*Leonotis nepetifolia* (*L. nepetifolia*) (L.) R.Br, also known as Lion's ear (Telugu name: Hanumantha Beera) or Christmas candlestick, was an

This is an open access article distributed under the terms of the Creative Commons Attribution-NonCommercial-ShareAlike 3.0 License, which allows others to remix, tweak, and build upon the work non-commercially, as long as the author is credited and the new creations are licensed under the identical terms

Accepted 14 February 2023

Revised 04 April 2022

Received 07 June 2021

Indian J Pharm Sci 2023;85(1):152-163

\*Address for correspondence

E-mail: parvataneni\_radhika@yahoo.com

economically important medicinal plant. It belonged to the family Lamiaceae and was widely used in Indian traditional medicinal systems<sup>[9,10]</sup>. The leaves decoction of this plant was used to treat burns cough and skin diseases. This plant has exhibited numerous pharmacological activities such as anti-inflammatory, anti-emetic, antimicrobial, wound healing, anti-diabetic, hepatoprotective, anticancer and anti-convulsant<sup>[11-14]</sup>. Recently, there was a report on the synthesis of AgNPs from aqueous dried leaf extract of *L. nepetifolia*<sup>[15]</sup>. The present investigation is the synthesis of AgNPs using aqueous fresh leaf extract of *L. nepetifolia* and evaluated their Antiproliferative activity on two human cancer cell lines for the first time.

## MATERIALS AND METHODS

### Materials:

All of the chemicals used for the experiments were analytical grade Silver nitrate purchased from Hi-Media Mumbai, India, and DMEM and RPMI media from Sigma-Aldrich (St. Louis, MO, United States of America (USA)). Polybutylene succinate was supplied by Sisco Research Laboratories Pvt. Ltd. (SRL), India. Fetal bovine serum was obtained from Gibco (Invitrogen), South America.

### Collection of plant material:

*L. nepetifolia* leaves were collected from Andhra University campus, Visakhapatnam, India. The plant was authenticated and identified by Prof. S. B. Padal, Taxonomist, Department of Botany, Andhra University, Visakhapatnam, with a voucher specimen number: 22287 deposited at Herbarium of Botany, Andhra University, Visakhapatnam, India.

### Crude leaf extracts preparation:

15 g of fresh *L. nepetifolia* leaves (wet weight) were weighed, properly cleaned with tap water and then washed with distilled water to remove dust particles. Mashed leaves were mixed with 50 ml of Milli-Q water and boiled for about 15 min. The aqueous leaf extract was filtered twice using Whatmann no.1 filter paper, and with a membrane (0.2 µm) was stored at 4° for further work. To perform Gas Chromatography-Mass Spectrometry (GC-MS) analysis, 250 g (wet weight) leaves of *L. nepetifolia* were weighed, cleaned with tap water, shade dried and powdered in a blender. The dried leaf powder, which weighed around 70 g (dry weight) was placed in a thimble and

extracted successively with ethanol using a Soxhlet extractor. The extracts were concentrated using a rotary flash evaporator.

Phytochemical evaluation of both *L. nepetifolia* aqueous and ethanolic leaf extracts was performed to detect the active phytoconstituent such as alkaloids, phenolics, flavonoids, steroids, terpenoids, coumarins, saponins, carbohydrates, cardiac glycosides, tannins, proteins and amino acids by using standard experimental protocols<sup>[16]</sup>.

### GC-MS Study:

A GC-MS study was conducted to investigate the phytochemical constituents of an ethanolic leaf extract of *L. nepetifolia* using a GC-MS equipment JEOL (Model: AccuTOF GCV). The following were the GC-MS system's experimental conditions; SE-54 non-polar capillary semi-standard column, 25 m, 0.31 mm ID, the mobile phase flow rate was set at 1.0 ml/min and the film thickness was 0.25 µm (carrier gas: He). The temperature of the oven was raised to 230° at 4 K/min in the gas chromatography portion, and the injection volume was 1.0 µl. The total GC running time was 35 min. The phytoconstituent were identified by comparing their mass spectra with those of available compounds in the NIST and Wiley libraries.

### Synthesis of AgNPs:

A typical reaction mixture containing 1 ml of *L. nepetifolia* aqueous leaf extract in 8 ml of 1 mM AgNO<sub>3</sub> was used to synthesize AgNPs at 80° in a boiling water bath for 90 min. Several optimization experiments (1:1, 1:2, 1:4, 1:6, 1:8, 1:10, 1:12 and 1:14) were conducted at room temperature to evaluate the optimal reaction ratio for AgNP synthesis and their stability<sup>[17]</sup>. All of the experiments were carried out in duplicates. The primary indication of AgNP synthesis was the golden yellow color in the colloidal reaction mixtures (1:12 and 1:14 at 24 h). The ratios 1:1, 1:2, 1:4, 1:6, 1:8, and 1:10 did not produce the same level of color transition even after 24 h. AgNPs require additional energy for bio reduction, as evidenced by the huge time lag.

To study the various factors influenced in the formation of the AgNPs, the concentration of the extract was 0.1 ml and the concentration of AgNO<sub>3</sub> was 0.8 ml to form a colloidal reaction mixture (1:8). The effect of temperature on AgNPs synthesis was examined by keeping the reaction mixture at different temperatures (50°, 60°, 70°, 80°, 90° and 100°). The effect of AgNO<sub>3</sub> was also monitored by increasing the AgNO<sub>3</sub>

concentration (1, 2, 3, 4 and 5 mM) with a constant volume of leaf extract. By keeping 1 mM AgNO<sub>3</sub> at a constant range, the effect of leaf extract concentration (0.1, 0.2, 0.3, 0.4 and 0.5 ml) was analyzed. Various buffers were used to evaluate the influence of pH (4-12) on AgNPs synthesis<sup>[18]</sup>. Furthermore, stability tests were conducted with and without a stabilizing agent. Following the experiment, the optimum concentration for bulk nano colloid preparation was identified. AgNPs were separated by centrifugation at 10 000 rpm for 15 min. The pellet was dispersed 2-3 times in Milli-Q water. Further, the characterization on the dried AgNPs was carried out.

### Characterization of AgNPs:

Ultra Violet-Visible (UV-Vis) spectroscopy (Shimadzu, UV-1800) in the range of 300-700 nm was used to confirm the biosynthesis of AgNPs. The characteristic optical properties of AgNPs were measured using UV-Vis spectroscopy. The particle surface morphology was determined by Field Emission Scanning Electron Microscopy (FESEM) (JOEL, JSM-7100F) at an accelerating voltage of 6 kV. AgNPs were coated on carbon tape and then identified. The purity and elemental composition of the AgNPs was determined using energy-dispersive X-Ray Spectroscopy (EDX), which was connected with FESEM. The morphological characteristics of the synthesized AgNPs were also investigated using a High-Resolution Transmission Electron Microscopy (HRTEM) on Tecnai G2, F30 HRTEM 300 kV. A drop coat of ultrasonically dispersed AgNPs were applied to the Transmission Electron Microscopy (TEM) grid and dried under a UV light for HRTEM analysis. To estimate the average particle size distribution, HRTEM images were processed using "ImageJ" software.

The size distribution by Polydispersity Index (PDI) and the zeta potential of the synthesized AgNPs measurements was obtained from the same instrument using a Zetasizer Ver. 7.13 (Malvern Panalytical, UK). The samples for ZP were placed in a disposable zeta cell at a temperature of 25°, with water as a dispersant, and repeated three times. X-Ray Diffraction (XRD) (PANalytical, X-Pert pro, Netherland) analysis was also performed to determine the crystalline nature of synthesized AgNPs. The functional groups involved in AgNPs biosynthesis and stability were screened using Fourier Transform Infrared Spectroscopy (FTIR) (Bruker IR) in 4000-400 cm<sup>-1</sup> by potassium bromide pelleting.

### Antiproliferative studies using sulforhodamine B assay:

Two human cancer cell lines, Pancreatic cancer cell line (PANC-1) and Ovarian cancer cell line (SK-OV-3) were selected for this study. The National Centre provided the cell lines for Cell Sciences in Pune, India. The cells were passaged using conventional trypsinization in Dulbecco's modified eagle medium, minimal essential medium, and Roswell park memorial institute medium containing glutamine. Cells were plated at a density of around 10 000 cells per well in a 96-well plate. Cells were treated in triplicates with different concentrations of *L. nepetifolia* AgNPs (LnAgNPs), *L. nepetifolia* Ethanolic Leaf Extract (LnELE) and commercially available synthetic AgNPs (10, 20, 40, 60, 80 and 100 µg/ml) and incubated for 48 h. Following the incubation period, cell monolayers were fixed in a 10 % trichloroacetic acid solution at 4° for 1 h, then washed with Milli-Q water to remove the trichloroacetic acid and dried. The excess dye was washed away with 1 % acetic acid after dried cell plates were stained for 30 min. The protein-bound dye was dissolved in a 10 mM Tris base solution. The Optical Density (OD) was measured at 510 nm in a Varioskan flash multimode reader (Thermo Scientific)<sup>[19,20]</sup>. Percent growth was calculated using the formula.

$$\text{Percentage growth} = \frac{\text{Average absorbance of the test}}{\text{Average absorbance of control}} \times 100$$

The acquired results in the Antiproliferative testing were indicated in Growth Inhibitory concentration (GI<sub>50</sub>) (Half-maximal inhibitory concentration (IC<sub>50</sub>)). The IC<sub>50</sub> value was determined as the drug concentration that causes a 50 % decrease in cell growth rate. Doxorubicin and Camptothecin (for ethanolic leaf extract of *L. nepetifolia* on SK-OV-3 cell lines)<sup>[21]</sup> were standard drugs used along with the synthesized biogenic AgNPs and synthetic AgNPs in this experiment.

### Statistical analysis:

The data were analyzed by one-way analysis of variance using Statistical Package for the Social Sciences (SPSS) software (IBM SPSS statistics-version 24). Data were presented as the mean±Standard Deviation (SD) of at least three separate variables, with a statistical level of p<0.001 being considered statistically significant.

## RESULTS AND DISCUSSION

The phytochemical analysis of aqueous and ethanolic leaf extracts showed the presence of phenols, flavonoids, steroids, terpenoids, saponins, carbohydrates and

amino acids. Alkaloids were absent. GC-MS data of ethanolic leaf extract revealed a total of 13 compounds shown in Table 1. Some of the compounds had simple ring structures like those reported in the literature but varied with different functional groups. The compounds were classified based on Retention Times (RT), and molecular structure. The GC-MS spectrum (fig. 1) showed. 9,12,15-Octadecatrienoic acid, ethyl ester, [Z, Z, Z]-, Hexadecanoic acid ethyl ester and 3,7,11,15-Tetramethyl-2-hexadecane-1-ol were the major compounds found in the ethanolic leaf extract. The RT with relative peak areas of the compounds were observed to be 25.15 (6.54 %), 22.11 (0.71 %) and 20.08 (0.75 %) respectively. Similar compounds such as Hexadecanoic acid, Octadecanoic acid, Linolenic acid, Eicosanoic acid, d-Mannitol and Squalene were found in the GC-MS analysis of genus *Ocimum* plants<sup>[22]</sup>. Hexadecanoic acid ethyl ester, 9,12,15-Octadecatrienoic acid, ethyl ester, [Z, Z, Z]-, and d-Mannitol, 1-decylsulfonyl- were found in the ethanolic leaf extracts of *Jatropha gossypifolia*<sup>[23]</sup>. 3,7,11,15-Tetramethyl-2-hexadecane-1-ol, 9,12,15-Octadecatrienoic acid, ethyl ester, Octadecanoic acid, and 2-Dodecen-1-yl (-) succinic anhydride found in the GC-MS analysis of hexane, diethyl ether and ethyl acetate fractions of

aerial parts of *Mollugo pentaphylla*<sup>[24]</sup>.

### Synthesis of AgNPs:

The reduction of silver ions ( $\text{Ag}^+$ ) into AgNPs ( $\text{Ag}^\circ$ ) through the bioactive compounds present in the *L. nepetifolia* aqueous leaf extract was known to exhibit specific optical properties due to Surface Plasmon Resonance (SPR), indicating the generation of AgNPs<sup>[25]</sup>. The reduction process of synthesized AgNPs was screened by UV-Vis spectroscopy, as shown in fig. 2.

The reaction time was optimized by keeping the reaction mixtures at room temperature and continuously monitored. OD values of these samples were taken at regular intervals by using UV-Vis spectroscopy and were shown in fig. 3a. The slower reduction rate of silver ions at room temperature was more likely due to variations in reduction. For  $\text{Ag}^+$  to  $\text{Ag}^\circ$ , the redox potential was much lower. Fewer AgNPs were formed with less color after 24 h. A broader peak was observed due to their low absorbance and stability, AgNPs were sedimented at the bottom of the tube with the increase in time<sup>[26]</sup>. The time required to complete the reaction varied depending on the reduction potential of plants, ranging from min to h<sup>[27]</sup>.

**TABLE 1: GC-MS ANALYSIS OF COMPOUNDS FROM ETHANOLIC CRUDE LEAF EXTRACT OF *L. nepetifolia* (L.)**

S. No	RT	Name of the compound	Molecular formula	Molecular weight	% Peak area	Type of Compound
1	3.51	Ethanol	$\text{C}_2\text{H}_6\text{O}$	46	0.04	Alcohol
2	20.08	3,7,11,15-Tetramethyl-2-hexadecan-1-ol	$\text{C}_{20}\text{H}_{40}\text{O}$	296	0.75	Diterpenoid
3	20.63	3,7,11,15-Tetramethyl-2-hexadecan-1-ol	$\text{C}_{20}\text{H}_{40}\text{O}$	296	0.49	Diterpenoid
4	22.11	Hexadecanoic acid, ethyl ester	$\text{C}_{18}\text{H}_{36}\text{O}_2$	284	0.71	Palmitic acid
5	23.97	9,12,15-Octadecatrienoic acid, ethyl ester, [Z,Z,Z]-	$\text{C}_{19}\text{H}_{32}\text{O}_2$	292	0.65	Linolenic acid ester compound
6	25.15	9,12,15-Octadecatrienoic acid	$\text{C}_{20}\text{H}_{34}\text{O}_2$	306	6.54	Linolenic acid
7	25.58	Octadecanoic acid, ethyl ester	$\text{C}_{20}\text{H}_{40}\text{O}_2$	312	0.60	Oleic acid ester
8	26.36	Octanoic acid, [1-methyl-3-(2,6,6-trimethyl cyclohex-1-enyl) propylenedene] hydrazide	$\text{C}_{21}\text{H}_{38}\text{N}_2\text{O}$	334	0.68	Medium chain fatty acid, carboxylic acid derivatives
9	27.95	2-Dodecen-1-yl (-) succinic anhydride	$\text{C}_{16}\text{H}_{26}\text{O}_3$	266	0.74	Carboxylic acid anhydride
10	28.5	Eicosanoic acid, ethyl ester	$\text{C}_{22}\text{H}_{44}\text{O}_2$	340	0.50	Long-chain fatty acid ethyl ester
11	30.89	d-mannitol, 1-decylsulfonyl	$\text{C}_{16}\text{H}_{34}\text{O}_7\text{S}$	370	0.67	Sugar alcohol with sulfur
12	32.17	1,4-Benzene diol, 2,6-bis (1,1-dimethylethyl)-	$\text{C}_{14}\text{H}_{22}\text{O}_2$	222	0.42	Alkyl benzene
13	33.52	Squalene	$\text{C}_{30}\text{H}_{50}$	410	0.35	Triterpenoid

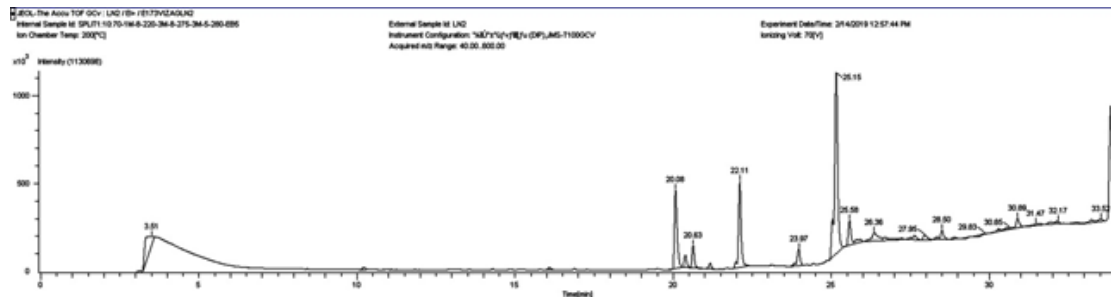


Fig. 1: GC-MS spectrum of ethanolic leaf extract of *L. nepetifolia*

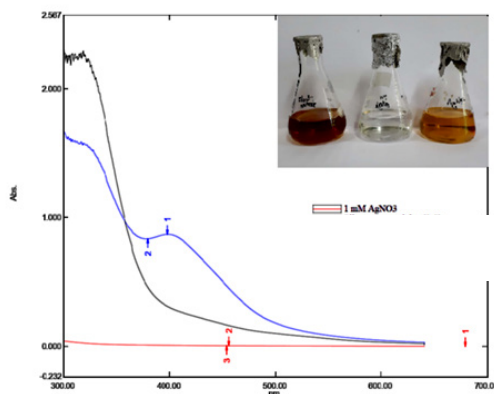


Fig. 2: UV-Vis spectra of *L. nepetifolia* mediated synthesis of AgNPs

Note: (—): 1mM AgNO<sub>3</sub>; (—): Silver nanoparticles 1:8 ratio of aqueous leaf extract of *L. nepetifolia* and 1 mM silver nitrate and (—): *L. nepetifolia* aqueous leaf extract

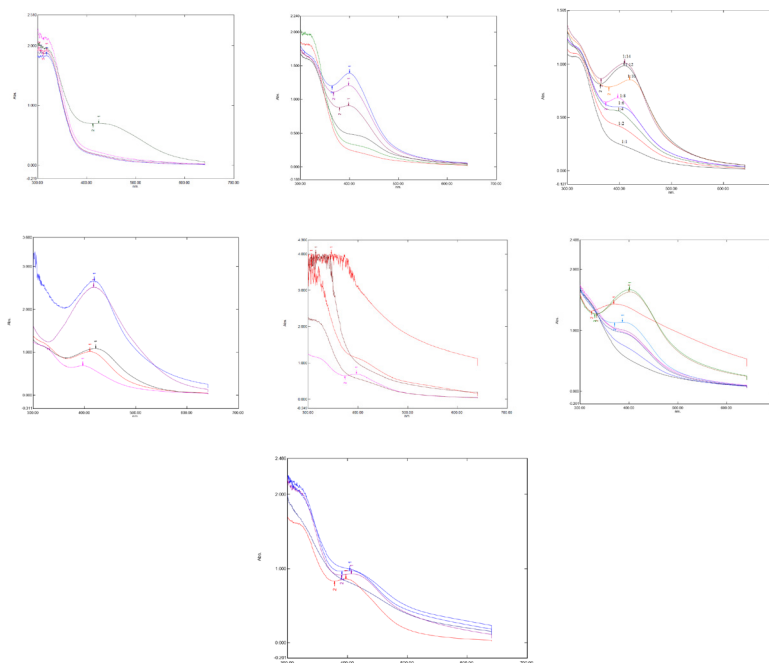


Fig. 3: UV-visible absorption spectra of optimized parameters for the synthesis of *L. nepetifolia* mediated AgNPs, (a): Effect of time (0 to 120 h) on AgNPs synthesis; (b): Effect of concentration of leaf extract and AgNO<sub>3</sub> (1:8) at different temperatures (50-100°C); (c): Different ratios (1:1 to 1:14) of leaf extract and AgNO<sub>3</sub> at 80°C; (d): Effect of different concentrations of AgNO<sub>3</sub> (1-5 mM); (e): Effect of different concentrations of leaf extract (0.1-0.5 ml); (f): Effect of different pH (4-12) and (g): Stability of AgNPs at room temperature

Note: (a): (no absorption): 0 h; (no absorption): 2 h; (no absorption): 24 h; (no absorption): 48 h and ( $\lambda$  max 425 nm): 5 d; (b): (no absorption): 50°C; (no absorption): 60°C; (no absorption): 70°C; ( $\lambda$  max 398 nm): 80°C; ( $\lambda$  max 400 nm): 90°C and ( $\lambda$  max 397 nm): 100°C; (c): (no absorption): 1:1; (no absorption): 1:2; (no absorption): 1:4; (no absorption): 1:6; ( $\lambda$  max 398 nm): 1:8; ( $\lambda$  max 419 nm): 1:10; ( $\lambda$  max 412 nm): 1:12 and ( $\lambda$  max 409 nm): 1:14; (d): ( $\lambda$  max 397 nm): 1 mM; ( $\lambda$  max 411 nm): 2 mM; ( $\lambda$  max 419 nm): 3 mM; ( $\lambda$  max 422 nm): 4 mM and ( $\lambda$  max 418 nm): 5 mM; (e): (no absorption): 0.1 ml; (absorption): 0.2 ml; (no absorption): 0.3 ml; (no absorption): 0.4 ml and (no absorption): 0.5 ml; (f): (no absorption): pH 4; (no absorption): pH 5; (no absorption): pH 6; (no absorption): pH 7; (no absorption): pH 8; ( $\lambda$  max 387 nm): pH 9; ( $\lambda$  max 402 nm): pH 10; ( $\lambda$  max 403 nm): pH 11 and (no absorption): pH 12 and (g): ( $\lambda$  max 397 nm): Day 1; ( $\lambda$  max 407 nm): Day 7; ( $\lambda$  max 404 nm): Day 14; (no absorption) Day 22 and (no absorption): Day 33

The optimized reaction mixtures containing test tubes were placed in a water bath with an interval of 10° rise in temperatures at 50°, 60°, 70°, 80°, 90° and 100°. There was no apparent increase in the size or number of AgNPs at 50°-70°. At higher incubation temperatures (80°-100°), an increase in color intensity and more extreme SPR peaks were revealed. The maximum SPR peak was detected at 398 nm at 80° for 90 min. As the temperature was increased, narrow peaks developed the smaller-sized nanoparticles (397 nm at 100°) in the lower wavelength region (fig. 3b and fig. 3c). AgNPs synthesized from aqueous fruit extract of *Terminalia chebula* had a similar SPR peak at 398 nm<sup>[28]</sup>, but this value differs from recently published aqueous leaf extract of *L. nepetifolia* at 420 nm<sup>[15]</sup>. The reactants were rapidly consumed when the temperature was raised, resulting in the formation of smaller nanoparticles. Similar results were observed when *Althaea officinalis* and *Citrullus lanatus* extracts were used as a reducing agent as the size of AgNPs decreased with an increase in temperature<sup>[29,30]</sup>.

At 0.1 ml of *L. nepetifolia* aqueous leaf extract and 0.8 ml of AgNO<sub>3</sub> at 80° for 90 min, the effect of AgNO<sub>3</sub> on AgNPs biosynthesis was studied in the range of 1 mM to 5 mM. The SPR peaks for AgNPs at various AgNO<sub>3</sub> concentrations were shown in fig. 3d. With an increase in AgNO<sub>3</sub> concentration in the solution for the specified reaction time, the color of the reaction mixture darkened and the size of nanoparticles was proportional to the color of the reaction mixture<sup>[31]</sup>. Similar results were observed for AgNPs synthesized from aqueous leaf extracts of *Impatiens balsamina*, *Lantana camara* and *Buddleja globosa* at different AgNO<sub>3</sub> concentrations. With increasing band intensity, the number of AgNPs in the reaction mixture increased<sup>[32,33]</sup>.

The concentration of aqueous leaf extract was optimized by changing the volume of *L. nepetifolia* aqueous leaf extract from 0.1 to 0.5 ml while keeping the other parameters kept constant (temperature and concentration of AgNO<sub>3</sub>). The number of nanoparticles in 0.2 ml of *L. nepetifolia* aqueous leaf extract was reported to be higher than in 0.1 ml<sup>[29]</sup>. This increased nucleation at a higher reductant volume would lead to a greater number of nanoparticles and a stronger SPR peak. The SPR band becomes more prominent and less concentrated with a blue shift in wavelength when the volume of *L. nepetifolia* aqueous leaf extract was increased from 0.3 to 0.5 ml (fig. 3e). Because there was more reductant available for the growth of stable nuclei than free Ag<sup>+</sup> ions, the reaction rate increased, resulting in a greater number of small-sized nanoparticles.

AgNPs shape, size, and stability were all affected by pH. Phosphate buffer (4,5,6), tris Hydrochloric acid, (7,8,9), and glycine-Sodium hydroxide (10,11,12) were the three buffer solutions used to carry out the reactions, which ranged in pH from 4 to 12. There was no color change or characteristic SPR peak in acidic conditions. The color intensity increased from golden yellow to reddish-orange as the solution became more alkaline. At alkaline pH, the formation of AgNPs was immediate, with an intense SPR peak observed at pH 10 (fig. 3f)<sup>[34]</sup>. Alkalinity enhanced the reduction and capping of AgNPs at various facets, as well as the subsequent deposition of silver atoms on these facets, at higher pH<sup>[35]</sup>. The functional groups responsible for reducing the precursor to nanoparticles possessed positive charges at acidic pH, lowering their reducing potential due to the large concentration of hydrogen ions.

AgNPs synthesized from the optimum reaction mixture (0.1 ml of *L. nepetifolia* aqueous leaf extract in 0.8 ml of 1 mM AgNO<sub>3</sub>) were studied for stability at 80° for 90 min, as shown in fig. 3g. The visual precipitation and the shift in SPR peak were considered when the stability of AgNPs was examined. The AgNPs were found to be stable in solution at room temperature even after 3 w of their synthesis (33 d) in the absence of the stabilizing agent<sup>[27]</sup>. The particles remained stable for 98 d at 4°. AgNPs sedimentation was observed at the tube's bottom, which was related to their overgrowth and agglomeration over time.

The stability of biologically synthesized nanoparticles was investigated in the presence of a stabilizing agent like Polyvinyl Pyrrolidone (PVP) aqueous solution (0.2 % and 0.5 %) was used. The concentration of PVP had a significant impact on the size distribution and dispersion of the resulting nanoparticles<sup>[36]</sup>. Particles were stable up to 45 d at room temperature and for more than 8 mo at 4°. At a concentration of 0.2 %, several agglomerated particles were observed. When the PVP concentration was increased (0.5 %), well-isolated mono dispersed nanoparticles of controlled size were synthesized.

### Characterization of AgNPs:

The morphology of the synthesized AgNPs was characterized using FESEM. An agglomeration of AgNPs was observed in the FESEM images (fig. 4a and fig. 4b). The AgNPs were formed spherical and polydispersed, which showed similarity with that of AgNPs in *Salvinia molesta* and wall nut husk were polydispersed and spherical in shape<sup>[37,38]</sup>. In EDX

spectra, a strong silver peak was recorded at 3 keV (fig. 4c). Apart from the silver signal, spectral signals for carbon and oxygen were also recorded.

The HRTEM images (fig. 5a and fig. 5b) showed a significant number of roughly spherical shaped AgNPs ranging in size from 2 to 38 nm. In the SAED pattern shown in fig. 5c, the bright circular rings revealed the crystalline nature of the synthesized AgNPs. The average size distribution of nanoparticles (11.32 nm) was defined by a size distribution histogram (fig. 5d), which was derived from several images of AgNPs corresponding to HRTEM, which showed similarity with that of an average size of 11.56 and 11 nm had been reported from leaf extracts of *Melaleuca alternifolia* and *Andrographis paniculata*<sup>[39,40]</sup>, but these values differ with that of recently reported AgNPs from *L. nepetifolia* (37.5 nm)<sup>[15]</sup>.

The PDI can be used to determine the size distribution of nanoparticles. The synthesized AgNPs had a PDI value of 0.44 that showed moderately dispersed, shown in fig. 6a. It was also reported that the AgNPs synthesized from the aqueous dried leaf extract of *L. nepetifolia*, dried wall nut (*Juglans regia*) husk, and flower extracts of *Aerva lanata* with PDI values of 0.48, 0.40 and 0.41<sup>[15,38,41]</sup>. A nanoparticle system with a PDI value greater than 0.4 and a value between 0.1 and 0.4 was found to have a highly polydispersed and moderately

dispersed distribution, in that order<sup>[42]</sup>. The zeta potential was a measure of the surface charge potential, which was a key factor for determining colloidal dispersion stability. The zeta potential value of synthesized AgNPs was shown in fig. 6b. Zeta potential values of the AgNPs were found to be  $-23.7 \pm 5.69$  mV, which is different from the reported value  $-12.3$  mV, but similar results of  $-23.1 \pm 0.6$  and  $-23.9$  mV were observed in the synthesis of the stable AgNPs from aqueous dried leaf extract, plant and aqueous leaf extracts of *L. nepetifolia*, *Ilex paraguariensis* and *Pterodon emarginatus*<sup>[15,43,44]</sup>.

The XRD spectrum of synthesized AgNPs revealed that four distinct diffraction peaks at  $2\theta = 38.38^\circ$ ,  $46.45^\circ$ ,  $67.63^\circ$ , and  $76.88^\circ$ , which corresponds to (111), (200), (220) and (311) with Face-Centered Cubic (FCC) structure and were similar with those recorded for the standard silver metal ( $\text{Ag}^\circ$ ) (JCPDS No. 00-04-0783, USA). XRD data obtained over a wide angular range of  $20^\circ \leq 2\theta \leq 80^\circ$ , revealed the crystalline nature of synthesized AgNPs shown in fig. 7. The diffraction peaks of LnAgNPs were similar with that of a polysaccharide<sup>[34]</sup> and the leaf extract of *Artemisia turcomanica*<sup>[8]</sup> mediated AgNPs ( $2\theta$  values  $38.1^\circ$ ,  $46.2^\circ$ ,  $67.4^\circ$ ,  $77.4^\circ$ ). The average crystallite size of the synthesized AgNPs was calculated using the Debye Scherrer equation

$$D = K\lambda/\beta \cos\theta \quad (1)$$

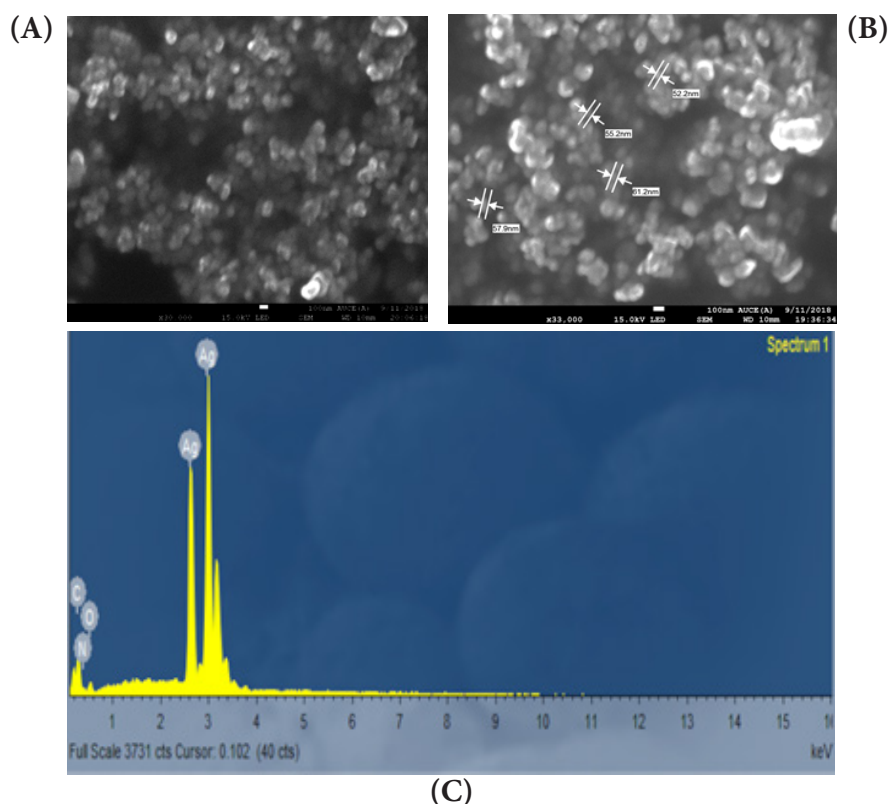


Fig. 4: (a and b): FESEM images of *L. nepetifolia* mediated AgNPs and (c): Corresponding EDX spectrum of AgNPs

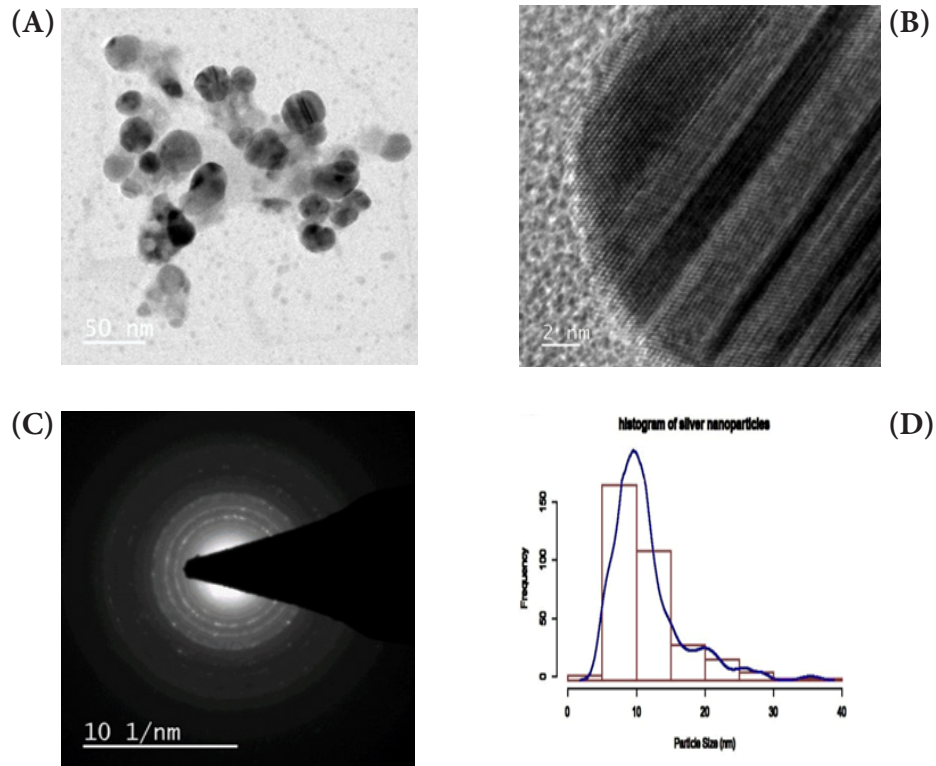


Fig. 5: (a and b): HRTEM micrographs of the *L. nepetifolia* mediated AgNPs; (c): SAED pattern and (d): Histogram of particle size distribution

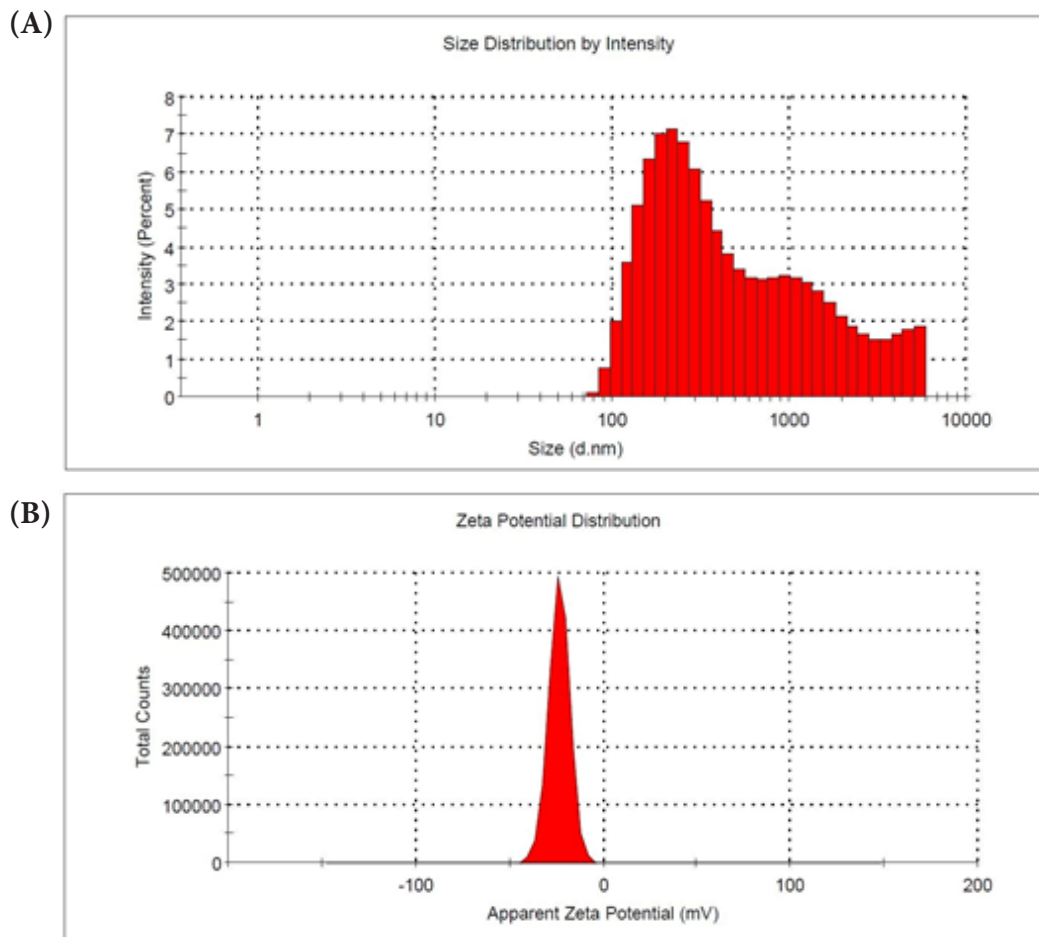


Fig. 6: (a): Polydispersity index graph of synthesized AgNPs and (b): Zeta potential distribution of AgNPs

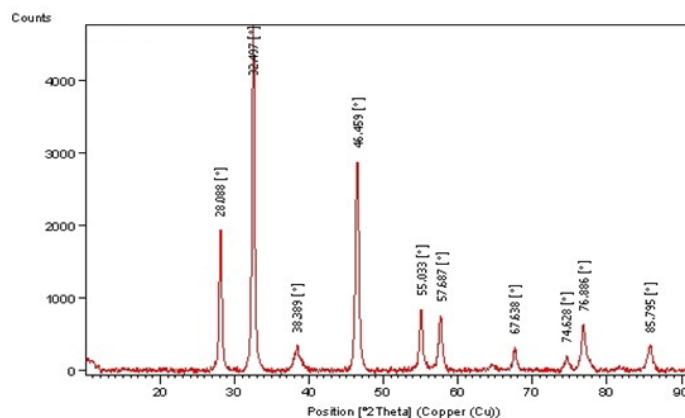


Fig. 7: X-ray diffractogram of *L. nepetifolia* mediated AgNPs

Where,  $D$  represents the average particle size,  $K$  represents the shape factor (constant 0.9),  $\lambda$  is the X-ray wavelength ( $1.5406 \text{ \AA}$ ),  $\beta$  is the full width at half maximum of the peak (FWHM), and  $\theta$  is the diffraction angle. The average crystallite size of the AgNPs synthesized by leaf extract of *L. nepetifolia* was 16.52 nm, comparable with that of the nearer value 11.32 nm obtained from TEM, but differs from the XRD value 8.5 nm observed from dried aqueous leaf extract of *L. nepetifolia*<sup>[15]</sup>.

FTIR analysis of *L. nepetifolia* aqueous leaf extract and its AgNPs was used to investigate the probable phytoconstituents present in *L. nepetifolia* aqueous leaf extract that were responsible for the synthesis and stability of AgNPs. *L. nepetifolia* leaf extract had notable bands at 3510.53, 3334.00, 2935.15, 1605.76, 1403.44, 1256.30 and 1077.44  $\text{cm}^{-1}$  in its FTIR spectra shown in fig 8a. The corresponding bands at 3334  $\text{cm}^{-1}$  ( $-\text{OH}$  and  $-\text{NH}$  stretching), 2935.15  $\text{cm}^{-1}$  ( $-\text{C}-\text{H}$  asymmetric stretching), 1605.76  $\text{cm}^{-1}$  ( $\text{C}=\text{O}$  stretching), 1403.44, 1256.30, 1077.44  $\text{cm}^{-1}$  ( $\text{C}-\text{O}-\text{C}$  and  $-\text{C}-\text{O}$  stretching). The FTIR spectrum of AgNPs showed a shift in the peaks, in contrast to the FTIR spectrum of *L. nepetifolia* leaf extract: from 3334.00 to 3169.77, 2935.15 to 2879.56, 1605.76 to 1639.86, 1403.44 to 1390.96, 1256.30 to 1233.74, 1077.44 to 1029.93, 777.22 to 778.67  $\text{cm}^{-1}$  (fig. 8b). According to these results, the amide, hydroxyl, carboxyl, and amino groups of phytoconstituents such as phenolic compounds, flavonoids, tannins, amino acids, and carbohydrates served as reducing and capping agents for the biosynthesis of AgNPs. Similar peaks (3135, 2926, 2933, 2857, 1631, 1608, 1407  $\text{cm}^{-1}$ ) were found in FTIR analysis of AgNPs synthesized from leaves and rhizome extracts of plants *Rhynchosia suaveolens*, *Camellia sinensis*, *Hibiscus rosasinensis* and *Coptidis*

*rhizome*<sup>[6,20,45,46]</sup>. The synthesis of AgNPs formation from plants was not clearly understood. These phytoconstituents could play a role in the reduction of silver salt solution ( $\text{Ag}^+-\text{Ag}^0$ ) and served as capping agents, resulted in stable AgNPs<sup>[47]</sup>. The possible synthesis of AgNPs from *L. nepetifolia* aqueous leaf extract was shown in fig. 9.

The SRB assay was a quantitative colorimetric method for determining cell survival and proliferation based on cellular protein content measurement. Since SRB binding was stoichiometric, the amount of bound dye was directly proportional to cell mass, allowing cell proliferation to be estimated. The anticancer activity of *Leontotis* mediated AgNPs LnAgNPs, LnELE, along with commercially available synthetic AgNPs was evaluated against human pancreatic (PANC-1) and ovarian cancer cell lines (SK-OV-3) respectively.

PANC-1 cell lines were treated with *L. nepetifolia* aqueous leaf extract mediated AgNPs, LnELE, and commercially available AgNPs with different concentrations (10,20,40,60,80,100  $\mu\text{g/ml}$ ) for 48 h. The cell viability decreased with an increase in nanoparticle concentration and significantly inhibited the proliferation of PANC-1 cell lines with an  $\text{IC}_{50}$  values of  $25.46 \pm 2.47$ ,  $43.89 \pm 13.29$ , and  $48.04 \pm 0.38$   $\mu\text{g/ml}$  (fig. 10), which were statistically significant ( $p < 0.001$ ), when compared with that of standard drug doxorubicin with  $\text{IC}_{50}$  value  $0.96 \pm 0.29$   $\mu\text{g/ml}$ . *L. nepetifolia* leaf extract mediated AgNPs were more potentially inhibited the proliferation of PANC-1 cancer cell lines than LnELE and commercially available AgNPs. Similar results were observed in a study on cytotoxic activity of Bangladesh medicinal plants on pancreatic cancer cell lines, especially *Amoora chittagonga* crude extract on PANC-1 cell lines, with  $\text{IC}_{50}$  values ranging between 42.8-49.8  $\mu\text{g/ml}$ <sup>[48]</sup>. The  $\text{IC}_{50}$  values of LnAgNPs were

not concurrent with that of AgNPs synthesized from sesquiterpenoids from *Tussilago farfara* flower bud extract on PANC-1 cell lines with an  $IC_{50}$  value of 166.1  $\mu$ M concentration<sup>[49]</sup>.

SK-OV-3 cell lines were treated with various concentrations of LnAgNPs, LnELE and commercially available AgNPs with different concentrations (10, 20, 40, 60, 80, 100  $\mu$ g/ml) for 48 h. The proliferation of SK-OV-3 cell lines was significantly inhibited with an  $IC_{50}$  value of  $23.93 \pm 2.3$ ,  $44.45 \pm 4.64$ , and  $42.04 \pm 0.62$   $\mu$ g/ml concentrations (fig. 11), which were statistically significant ( $p < 0.001$ ) when compared to the standard drugs doxorubicin and Camptothecin with an  $IC_{50}$  values of  $2.93 \pm 0.49$  and  $2.82$   $\mu$ g/ml. LnAgNPs had exhibited high Antiproliferative activity over that of the LnELE and commercially available AgNPs. The aqueous leaf extracts of *Rhynchosia suaveolens* and *Gloriosa superba* mediated AgNPs showed potent cytotoxic activity ( $IC_{50}$ ) of 4.2 and  $61.80 \pm 4.27$   $\mu$ g/ml on SK-OV-3 cell lines<sup>[6,50]</sup>. Further, it was reported that the ethanolic leaf extract of *Ocimum basilicum* showed cytotoxicity at a concentration of 5 mg/ml within 72 h with an  $IC_{50}$  value of  $0.91 \pm 0.11$  mg/ml on SK-OV-3 cell

lines<sup>[51]</sup>.

In conclusion, the eco-friendly synthesis of AgNPs was a cost-effective and non-toxic process. In the present study, AgNPs were synthesized using an aqueous leaf extract of *L. nepetifolia*. Phytochemical analysis and GC-MS data revealed that the aqueous and ethanolic leaf extracts of *L. nepetifolia* were rich in various phytochemical constituents acting as reducing and capping agents in AgNPs synthesis. The effect of various physicochemical factors (0.1 ml leaf extract, 1 mM  $AgNO_3$  at  $80^\circ$  at pH 10) was recorded, and the synthesized AgNPs were stable up to 33 d at room temperature. The synthesized AgNPs were spherical in shape, with an average particle size of 11.32 nm, PDI 0.44, zeta potential  $-23.7 \pm 5.69$  mv, and crystalline in nature. A comparative cytotoxic study was done for synthesized AgNPs and commercially available AgNPs and found to be statistically significant. Biogenic nanoparticles showed concentration-dependent activity on human cancer cell lines PANC-1 and SK-OV-3 and inhibited the proliferation of both more effectively than synthetic AgNPs.

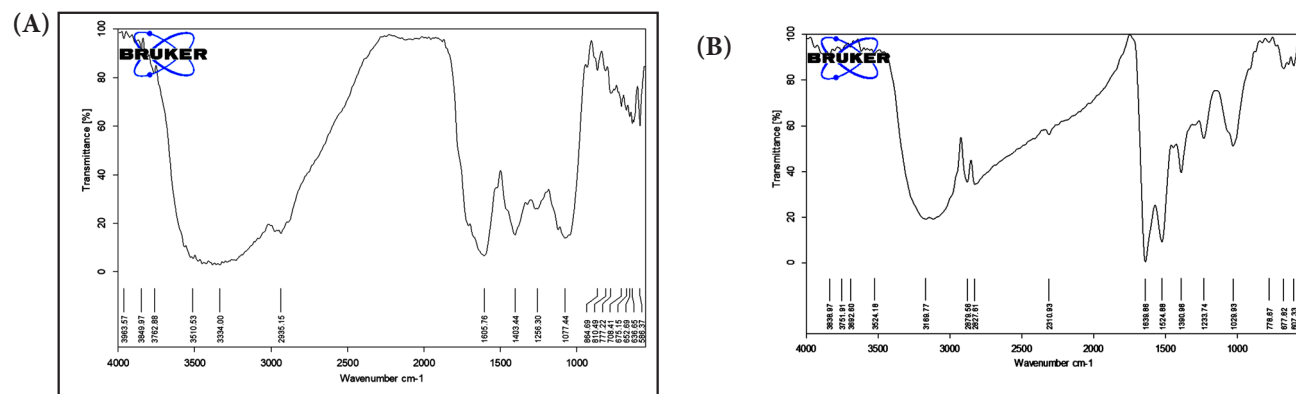
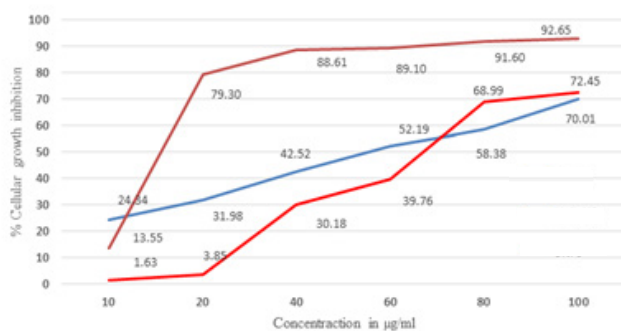


Fig. 8: FTIR spectra of (a): *L. nepetifolia* aqueous leaf extract and (b): *L. nepetifolia* mediated AgNPs

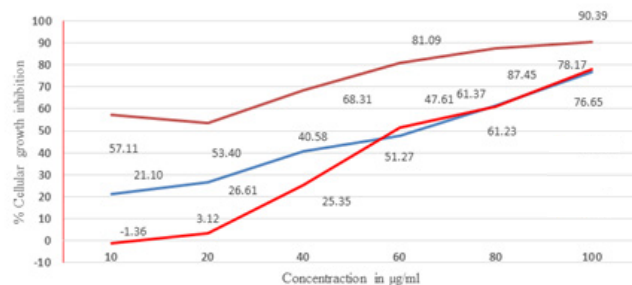


Fig. 9: Possible synthesis of AgNPs from aqueous leaf extract of *L. nepetifolia*



**Fig. 10:** Comparison of antiproliferative activity of *L. nepetifolia* AgNPs, *L. nepetifolia* ethanolic leaf extract (LnELE) and SNPs for PANC-1 cell lines

Note: (—): LnELE; (—): LnAgNPs and (—): SNPs



**Fig. 11:** Comparison of antiproliferative activity of *L. nepetifolia* AgNPs, *L. nepetifolia* ethanolic leaf extract (LnELE) and SNPs for SK-OV-3 cell lines

Note: (—): LnELE; (—): LnAgNPs and (—): SNPs

### Acknowledgment:

We acknowledge UGC, New Delhi (Ref No. 42-376/2013 (SR)), provided financial support for a period of 3 y. The authors are thankful to the Advanced Analytical Laboratory (DST) and Centre of Nanotechnology, Andhra University, Visakhapatnam, for providing XRD and FESEM data. The authors are thankful to SAIF, IIT Bombay, CSIR-Indian Institute of Chemical Technology, and Lavin Laboratories, Hyderabad, for providing HRTEM, GC-MS, PDI, zeta potential, and cytotoxicity data.

### Conflict of interests:

The authors declare no conflict of interests.

### REFERENCES

- Zottel A, Videtič Paska A, Jovčevska I. Nanotechnology meets oncology: Nanomaterials in brain cancer research, diagnosis and therapy. *Materials* 2019;12(10):1588.
- Wypij M, Jędrzejewski T, Trzczińska-Wencel J, Ostrowski M, Rai M, Golińska P. Green synthesized silver nanoparticles: Antibacterial and anticancer activities, biocompatibility, and analyses of surface-attached proteins. *Front Microbiol* 2021;12:632505.
- Wang Z, Lee S, Koo KI, Kim K. Nanowire-based sensors for biological and medical applications. *IEEE Trans Nanobiosci*

- 2016;15(3):186-99.
- Chatterjee B, Das SJ, Anand A, Sharma TK. Nanozymes and aptamer-based biosensing. *Mat Sci Energy Technol* 2020;3:127-35.
- Colapicchioni V, Millozzi F, Parolini O, Palacios D. Nanomedicine, a valuable tool for skeletal muscle disorders: Challenges, promises, and limitations. *Wiley Interdiscip Rev Nanomed Nanobiotechnol* 2022;14(3):e1777.
- Bethu MS, Netala VR, Domdi L, Tartte V, Janapala VR. Potential anticancer activity of biogenic silver nanoparticles using leaf extract of *Rhynchosia suaveolens*: An insight into the mechanism. *Artif Cells Nanomed Biotechnol* 2018;46(1):104-14.
- Plackal Adimuriyil George B, Kumar N, Abrahamse H, Ray SS. Apoptotic efficacy of multifaceted biosynthesized silver nanoparticles on human adenocarcinoma cells. *Sci Rep* 2018;8(1):14368.
- Mousavi B, Tafvizi F, Zaker Bostanabad S. Green synthesis of silver nanoparticles using *Artemisia turcomanica* leaf extract and the study of anti-cancer effect and apoptosis induction on gastric cancer cell line (AGS). *Artif Cell Nanomed Biotechnol* 2018;46(1):499-510.
- Vasuki K, Kokila Priya S, Nandini P, Pavithra U, Kiruthika G. Pharmacological properties of *Leonotis nepetifolia* (L.) R.BR-A short review. *Ayushdhara* 2015;2:162-166.
- Pushpan R, Nishteswar K, Kumari H. Ethno medicinal claims of *Leonotis nepetifolia* (L.) R. BR: A review. *Int J Res Ayurveda Pharm* 2012;3(5).
- Kamalam M, Saraswathi C, Umadevi U. Evaluation of *Leonotis nepetaefolia* for its phytochemical and heavy metal analysis. *Int J Pharm Sci Res* 2013;4(12):4591-6.
- Kumar BJ, Kumar RS, Deepthi R, Bakshi V. Phytochemical screening and anti-emetic activity of *Leonotis nepetifolia* leaves extract. *Int J Pharm Chem* 2016;6(7):177-80.
- Veerabadrhan U, Venkatraman A, Souprayane A, Narayanasamy M, Perumal D, Elumalai S, *et al.* Evaluation of antioxidant potential of leaves of *Leonotis nepetifolia* and its inhibitory effect on MCF7 and Hep2 cancer cell lines. *Asian Pac J Trop Dis* 2013;3(2):103-10.
- Williams AF, Clement YN, Nayak SB, Rao AV. *Leonotis nepetifolia* protects against acetaminophen-induced hepatotoxicity: Histological studies and the role of antioxidant enzymes. *Nat Prod Chem Res* 2016;4(222):2.
- Manimegalai T, Raguvaran K, Kalpana M, Maheswaran R. Green synthesis of silver nanoparticle using *Leonotis nepetifolia* and their toxicity against vector mosquitoes of *Aedes aegypti* and *Culex quinquefasciatus* and agricultural pests of *Spodoptera litura* and *Helicoverpa armigera*. *Env Sci Poll Res* 2020;27(34):43103-16.
- Trease EG, Evans WC. *Textbook of Pharmacognosy*. 14<sup>th</sup> ed. UK: WB Saunders Company; 1997. p. 119.
- Ningrum AS, Pridyantari AP, Handayani W, Secario K, Djuhana D, Imawan C. Green synthesis of silver nanoparticles using leaf and stem bark extract of *Pometia pinnata* JR Forst & G. Forst. *Conf Ser Earth Environ Sci* 2020;481(1):012018.
- Cicek S, Gungor AA, Adiguzel A, Nadaroglu H. Biochemical evaluation and green synthesis of nano silver using peroxidase from *Euphorbia* (*Euphorbia amygdaloides*) and its antibacterial activity. *J Chem* 2015;2015:1-7.
- Vichai V, Kirtikara K. Sulforhodamine B colorimetric assay for cytotoxicity screening. *Nat Protoc* 2006;1(3):1112-6.
- Yadav A, Mendhulkar VD. Antiproliferative activity of *Camellia sinensis* mediated silver nanoparticles on three different human cancer cell lines. *J Cancer Res Ther* 2018;14(6):1316-24.

21. Zhou Z, Piao Y, Hao L, Wang G, Zhou Z, Shen Y. Acidity-responsive shell-sheddable camptothecin-based nanofibers for carrier-free cancer drug delivery. *Nanoscale* 2019;11(34):15907-16.
22. Chowdhury T, Mandal A, Roy SC, De Sarker D. Diversity of the genus *Ocimum* (Lamiaceae) through morpho-molecular (RAPD) and chemical (GC-MS) analysis. *J Genet Eng Biotechnol* 2017;15(1):275-86.
23. Bharathy V, Sumathy BM, Uthayakumari F. Determination of phytochemicals by GC-MS in leaves of *Jatropha gossypifolia* L. *Sci Res Rep* 2012;2(3):286-90.
24. Niyogi P, Pattnaik S, Maharana L. Quantitative Identification of Major and Minor Constituents of Aerial Parts of *Mollugo pentaphylla* Linn. using GC-MS. *Asian J Chem* 2016;28(10):2335.
25. Mulvaney P. Surface plasmon spectroscopy of nanosized metal particles. *Langmuir* 1996;12(3):788-800.
26. Niluxshun MC, Masilamani K, Mathiventhan U. Green synthesis of silver nanoparticles from the extracts of fruit peel of *Citrus tangerina*, *Citrus sinensis*, and *Citrus limon* for antibacterial activities. *Bioinorg Chem Appl* 2021;2021.
27. Shankar SS, Rai A, Ahmad A, Sastry M. Rapid synthesis of Au, Ag, and bimetallic Au core-Ag shell nanoparticles using Neem (*Azadirachta indica*) leaf broth. *J Colloid Interface Sci* 2004;275(2):496-502.
28. Kirthika P, Dheeba B, Sivakumar R. Plant mediated synthesis and characterization of silver nanoparticles. *Int J Pharm Pharm Sci* 2014;6(8):304-10.
29. Rheder DT, Guilger M, Bilesky-José N, Germano-Costa T, Pasquoto-Stigliani T, Gallep TB, *et al.* Synthesis of biogenic silver nanoparticles using *Althaea officinalis* as reducing agent: Evaluation of toxicity and ecotoxicity. *Sci Rep* 2018;8(1):12397.
30. Ndikau M, Noah NM, Andala DM, Masika E. Green synthesis and characterization of silver nanoparticles using *Citrullus lanatus* fruit rind extract. *Int J Anal Chem* 2017;2017:8108504.
31. Mock JJ, Barbic M, Smith DR, Schultz DA, Schultz S. Shape effects in plasmon resonance of individual colloidal silver nanoparticles. *J Chem Phys* 2002;116(15):6755-9.
32. Aritonang HF, Koleangan H, Wuntu AD. Synthesis of silver nanoparticles using aqueous extract of medicinal plants (Impatiens balsamina and Lantana camara) fresh leaves and analysis of antimicrobial activity. *Int J Microbiol* 2019;2019.
33. Carmona ER, Benito N, Plaza T, Recio-Sánchez G. Green synthesis of silver nanoparticles by using leaf extracts from the endemic *Buddleja globosa* hope. *Green Chem Lett Rev* 2017;10(4):250-6.
34. Skiba MI, Vorobyova VI, Pivovarov A, Makarshenko NP. Green synthesis of silver nanoparticles in the presence of polysaccharide: Optimization and characterization. *J Nanomater* 2020;2020:1-10.
35. Sumi Maria B, Devadiga A, Shetty Kodialbail V, Saidutta MB. Synthesis of silver nanoparticles using medicinal *Zizyphus xylopyrus* bark extract. *Appl Nanosci* 2015;5(6):755-62.
36. Malina D, Sobczak-Kupiec A, Wzorek Z, Kowalski Z. Silver nanoparticles synthesis with different concentrations of polyvinylpyrrolidone. *Dig J Nanomater Biostruct* 2012;7(4):1527-34.
37. Verma DK, Hasan SH, Banik RM. Photo-catalyzed and phyto-mediated rapid green synthesis of silver nanoparticles using herbal extract of *Salvinia molesta* and its antimicrobial efficacy. *J Photochem Photobiol B* 2016;155:51-9.
38. Khorrami S, Zarrabi A, Khaleghi M, Danaei M, Mozafari MR. Selective cytotoxicity of green synthesized silver nanoparticles against the MCF-7 tumor cell line and their enhanced antioxidant and antimicrobial properties. *Int J Nanomed* 2018;13:8013-24.
39. Ramadan MA, Shawkey AE, Rabeh MA, Abdellatif AO. Promising antimicrobial activities of oil and silver nanoparticles obtained from *Melaleuca alternifolia* leaves against selected skin-infecting pathogens. *J Herb Med* 2020;20:100289.
40. Yadav S, Sharma S, Ahmad F, Rathaur S. Antifilarial efficacy of green silver nanoparticles synthesized using *Andrographis paniculata*. *J Drug Deliv Sci Technol* 2020;56:101557.
41. Palithya S, Gaddam SA, Kotakadi VS, Penchalaneni J, Golla N, Krishna SB, *et al.* Green synthesis of silver nanoparticles using flower extracts of *Aerva lanata* and their biomedical applications. *Part Sci Technol* 2022;40(1):84-96.
42. Ardani HK, Imawan C, Handayani W, Djuhana D, Harmoko A, Fauzia V. Enhancement of the stability of silver nanoparticles synthesized using aqueous extract of *Diospyros discolor* Willd. leaves using polyvinyl alcohol. *Conf Ser: Mater Sci Eng* 2017;188(1):012056.
43. Silveira AP, Bonatto CC, Lopes CA, Rivera LM, Silva LP. Physicochemical characteristics and antibacterial effects of silver nanoparticles produced using the aqueous extract of *Ilex paraguariensis*. *Mater Chem Phys* 2018;216:476-84.
44. Oliveira GZ, Lopes CA, Sousa MH, Silva LP. Synthesis of silver nanoparticles using aqueous extracts of *Pterodon emarginatus* leaves collected in the summer and winter seasons. *Int Nano Lett* 2019;9:109-17.
45. Singh A, Gaud B, Jaybhaye S. Optimization of synthesis parameters of silver nanoparticles and its antimicrobial activity. *Mater Sci Energy Technol* 2020;3:232-6.
46. Sharma G, Nam JS, Sharma AR, Lee SS. Antimicrobial potential of silver nanoparticles synthesized using medicinal herb *Coptidis rhizome*. *Molecules* 2018;23(9):2268.
47. Ovais M, Khalil AT, Islam NU, Ahmad I, Ayaz M, Saravanan M, *et al.* Role of plant phytochemicals and microbial enzymes in biosynthesis of metallic nanoparticles. *Appl Microbiol Biotechnol* 2018;102(16):6799-814.
48. George S, Bhalerao SV, Lidstone EA, Ahmad IS, Abbasi A, Cunningham BT, *et al.* Cytotoxicity screening of Bangladeshi medicinal plant extracts on pancreatic cancer cells. *BMC Complement Altern Med* 2010;10(1):52.
49. Lee YJ, Song K, Cha SH, Cho S, Kim YS, Park Y. Sesquiterpenoids from *Tussilago farfara* flower bud extract for the eco-friendly synthesis of silver and gold nanoparticles possessing antibacterial and anticancer activities. *Nanomaterials* 2019;9(6):819.
50. Bethu MS, Rao JV. Biofabrication of silver nanoparticles using leaves of *Gloriosa superba* and its anticancer properties. *Asian J Pharm Clin Res* 2017;10(11):65-9.
51. Hanachi P, Fakhreznhad FR, Zarringhalami R, Orhan IE. Cytotoxicity of *Ocimum basilicum* and *Impatiens walleriana* extracts on AGS and SKOV-3 cancer cell lines by flow cytometry analysis. *Int J Cancer Management* 2021;14(3):1-8.